Advanced Robotics, Vol. 19, No. 5, pp. 613–634 (2005)
© VSP and Robotics Society of Japan 2005.
Also available online - www.vsppub.com

Downloaded by [Botswana International University of Science & Technology (BIUST)] at 03:34 20 October 2017

Full paper

Compliant motion using a mobile manipulator: an operational space formulation approach to aircraft canopy polishing

RODRIGO S. JAMISOLA, JR. [1], DENNY N. OETOMO [2], MARCELO H. ANG, JR. [2,*], OUSSAMA KHATIB [3], TAO MING LIM [4] and SER YONG LIM [4]

[1] *Department of Electrical Engineering, Colorado State University, fort Collins, CO, USA*
[2] *Department of Mechanical Engineering, National University of Singapore, Singapore*
[3] *Computer Science Department, Stanford University, Stanford, CA, USA*
[4] *Singapore Institute of Manufacturing Technology, Singapore*

Received 30 July 2004; accepted 23 December 2004

Abstract—The operational space formulation provides a framework for the analysis and control of robotic systems with respect to interactions with their environments. In this paper, we discuss its implementation on a mobile manipulator programmed to polish an aircraft canopy with a curved surface of unknown geometry. The polishing task requires the robot to apply a specified normal force on the canopy surface while simultaneously performing a compliant motion keeping the surface of the grinding tool tangentially in contact with the workpiece. A human operator controls the mobile base *via* a joystick to guide the polishing tool to desired areas on the canopy surface, effectively increasing the mobile manipulator's reachable workspace. The results demonstrate the efficacy of compliant motion and force regulation based on the operational space formulation for robots performing tasks in unknown environments with robustness towards base motion disturbances. The mobile manipulator consists of a PUMA 560 arm mounted on top of a Nomad XR4000 mobile base. Implementation issues are discussed and experimental results are shown.

Keywords: Operational space formulation; canopy polishing; simultaneous force and motion control; mobile manipulator; compliant motion.

1. INTRODUCTION

Robust interaction between a robot and its environment is one of the most important goals of robotic systems. This is dependent on the robot's dexterity to simultaneously execute a desired motion and apply a desired force to its environment. The

*To whom correspondence should be addressed. E-mail: mpeangh@nus.edu.sg

Figure 1. A mobile manipulator consisting of a PUMA 560 mounted on a Nomad XR4000 polishing an aircraft canopy with a curved surface geometry that is unknown to the mobile manipulator. The polishing tool attached to the arm end-effector moves in a compliant scrubbing motion while maintaining a desired normal force on the aircraft canopy. The mobile base is guided by the human operator to polish the to desired areas on the canopy surface.

environment could be known to the robot, or completely unknown and unstructured, or it could even be dynamically changing. The robustness of a robot in a dynamically changing environment remains a challenge to this day.

A significant number of studies have been dedicated to the simultaneous force and motion control strategies. These studies can be divided into two categories [1]. The first category is characterized by a force control along the direction constrained by the environment and a motion control along the direction of free motion [2–4] where compliance can be achieved as shown in Refs [5–7]. The second category is characterized by achieving a desired force through a robot end-effector position control [8–11].

Among the many known algorithms, the operational space formulation by Khatib [3, 12] provides a complete treatment of the force and motion control of a robot end-effector along orthogonal directions. In this paper, an interesting application of the operational space formulation in the maintenance of aircraft canopies is shown. The aircraft canopies are polished to remove scratches and other imperfections. This task is typically done manually by human operators and is a very tedious process. In this work, attempts are made to assist human operators, through a mobile manipulator, in the aircraft canopy polishing task in order to achieve increased accuracy and productivity. The curved surface geometry of the aircraft canopy is unknown to the mobile manipulator. The tool, in the form of a polishing (or grinding) tool is attached to the end-effector of the manipulator. The tool is programmed to move in a scrubbing motion compliant to the canopy surface while maintaining a desired normal force. A human operator moves the base of the mobile manipulator, *via* a joystick, while the robot arm is autonomously performing the polishing task, thereby increasing its workspace and allowing the mobile manipulator to polish the entire surface of the canopy. Figure 1 shows the mobile manipulator used in this

Downloaded by [Botswana International University of Science & Technology (BIUST)] at 03:34 20 October 2017

Downloaded by [Botswana International University of Science & Technology (BIUST)] at 03:34 20 October 2017

work. It consists of a PUMA 560 articulated arm mounted on a Nomad XR4000 omni-directional mobile base.

This paper demonstrates the robustness of the operational space formulation to achieve simultaneous force and motion control tasks, despite the motion of the mobile base (that is treated as disturbance) and the unknown contact geometries. A method of handling robot arm singularities is also integrated into the algorithm, allowing smooth motion through singular configurations while doing the required polishing motion and maintaining the desired normal force. This is necessary as the wrist singularity of PUMA 560 is located at the position when the wrist is straightened, which is an easily reached configuration, resulting in a considerable loss of usable workspace. Impact control achieves a stable transition from free to constrained motion as the robot end-effector approaches and comes into contact with the canopy surface. Throughout the polishing task, instantaneous normal force exerted on the aircraft canopy was maintained at 10 ± 4 N with the base moving at approximately 0.5 m/s, and with the robot arm going in and out of singular configurations.

While the system can autonomously perform the force and motion control of the polishing tool on the surface of the canopy, a human operator is placed in the loop to provide the high-level commands such as which part of the workpiece needs more polishing or the polishing trajectory the tool should follow due to the irregular shape of the canopy. Placing the human operator in the loop can be done with a joystick, or even with a haptic device, as described in Ref. [13]. This is an example of an emerging paradigm for robotic applications where man–robot systems operate together with 'divided intelligence': humans provide high-level commands such as deciding which part of the workpiece needs more polishing or choosing the trajectory that the polishing tool should follow without providing details of intricate motions, the robot autonomously does the polishing using compliant motion. Here, the human operator and the robot do their respective tasks by exploiting their individual strengths and capabilities. The skill required for manual polishing is removed from experienced human operators and transferred to the robot, hence we also refer to this as 'de-skilling'.

This paper is organized as follows. Section 2 provides a review of the operational space formulation. Singularity handling, impact control and friction are also discussed in this section. Implementation details including choosing the operational space control point and frame is discussed in Section 3. Section 4 presents the implementation results. Section 5 summarizes this work and discusses some issues for future implementation.

2. THE OPERATIONAL SPACE FORMULATION

The operational space formulation [3, 12] describes the dynamics of the robot as seen at the end-effector. Motion of the end-effector is generated as the necessary force vector from the current position and orientation to the desired. This establishes

Downloaded by [Botswana International University of Science & Technology (BIUST)] at 03:34 20 October 2017

a unified approach to force and motion control and is a direct and natural way of expressing a manipulator's dynamic interaction with its environment. However, knowledge of the robot dynamics is required to fully realize the benefits.

The operational space is defined by a Cartesian coordinate frame attached to the end-effector where a direct interaction between the robot and its environment takes place. Motion of the end-effector and forces acting on it, including forces induced by the mobile manipulator's dynamics, are expressed in the operational space.

The motion of the end-effector in the operational space can be expressed as

$$\mathbf{F}_{\text{motion}} = \hat{\mathbf{\Lambda}}(\mathbf{x})\mathbf{F}^{*}_{\text{motion}} + \hat{\boldsymbol{\mu}}(\mathbf{x}, \dot{\mathbf{x}}) + \hat{\mathbf{p}}(\mathbf{x}). \tag{1}$$

The symbol $\hat{\mathbf{\Lambda}}(\mathbf{x})$ denotes the inertia matrix, $\hat{\boldsymbol{\mu}}(\mathbf{x}, \dot{\mathbf{x}})$ denotes the Coriolis and centrifugal forces, $\hat{\mathbf{p}}(\mathbf{x})$ denotes the gravitational forces, $\mathbf{x}$ denotes displacement and $\dot{\mathbf{x}}$ denotes velocity. All these parameters are expressed in the operational space. A physical parameter with a caret symbol ($\hat{}$) above it indicates that an estimate of this parameter is used. The symbol $\mathbf{F}^{*}_{\text{motion}}$ denotes the operational space motion control law and can be expressed as

$$\mathbf{F}^{*}_{\text{motion}} = \ddot{\mathbf{x}}_{\text{d}} - \mathbf{k}_{\text{v\_motion}}(\dot{\mathbf{x}} - \dot{\mathbf{x}}_{\text{d}}) - \mathbf{k}_{\text{p\_motion}}(\mathbf{x} - \mathbf{x}_{\text{d}}), \tag{2}$$

where $\ddot{\mathbf{x}}_{\text{d}}$, $\dot{\mathbf{x}}_{\text{d}}$ and $\mathbf{x}_{\text{d}}$ denote the desired acceleration, velocity and displacement of the end-effector, respectively; and $\mathbf{k}_{\text{p\_motion}}$ and $\mathbf{k}_{\text{v\_motion}}$ denote proportional and derivative gains for motion control, respectively.

The physical parameters in the operational space are derived from the joint space parameters using:

$$\begin{aligned} \hat{\mathbf{\Lambda}}(\mathbf{x}) &= \left[\mathbf{J}(\mathbf{q})\,\hat{\mathbf{A}}^{-1}(\mathbf{q})\,\mathbf{J}^{\text{T}}(\mathbf{q})\right]^{-1}, \\ \hat{\boldsymbol{\mu}}(\mathbf{x}, \dot{\mathbf{x}}) &= \mathbf{J}^{-\text{T}}(\mathbf{q})\,\hat{\mathbf{c}}(\mathbf{q}, \dot{\mathbf{q}}) - \hat{\mathbf{\Lambda}}(\mathbf{x})\,\dot{\mathbf{J}}(\mathbf{q})\,\dot{\mathbf{q}}, \\ \hat{\mathbf{p}}(\mathbf{x}) &= \mathbf{J}^{-\text{T}}(\mathbf{q})\,\hat{\mathbf{g}}(\mathbf{q}), \end{aligned} \tag{3}$$

where $\mathbf{J}(\mathbf{q})$ denotes the manipulator Jacobian matrix, $\hat{\mathbf{A}}(\mathbf{q})$ denotes the inertia matrix, $\hat{\mathbf{c}}(\mathbf{q}, \dot{\mathbf{q}})$ denotes the Coriolis and centrifugal forces, $\hat{\mathbf{g}}(\mathbf{q})$ denotes the gravitational forces, $\mathbf{q}$ denotes joint displacement and $\dot{\mathbf{q}}$ denotes joint velocity. All these are expressed in the joint space.

The force experienced at the end-effector as it interacts with its environment in the operational space can be expressed as

$$\mathbf{F}_{\text{force}} = \hat{\mathbf{\Lambda}}(\mathbf{x})\mathbf{F}^{*}_{\text{force}} + \hat{\boldsymbol{\mu}}(\mathbf{x}, \dot{\mathbf{x}}) + \hat{\mathbf{p}}(\mathbf{x}) + \mathbf{f}_{\text{d}}, \tag{4}$$

where $\mathbf{f}_{\text{d}}$ is the desired force applied by the end-effector on the environment. Of equal magnitude and in the opposite direction is the desired force applied by the environment on the operational point. The symbol $\mathbf{F}^{*}_{\text{force}}$ denotes the operational space force control law and can be expressed as

$$\mathbf{F}^{*}_{\text{force}} = \mathbf{k}_{\text{p\_force}}(\mathbf{f}_{\text{d}} - \mathbf{f}) + \mathbf{k}_{\text{i\_force}} \int (\mathbf{f}_{\text{d}} - \mathbf{f}). \tag{5}$$

Downloaded by [Botswana International University of Science & Technology (BIUST)] at 03:34 20 October 2017

The actual force exerted by the end-effector on its environment, denoted **f**, is derived from the force/torque sensor reading by taking the negative of the force that is read from the sensor. The direct force sensor feedback is the actual force exerted by the environment on the end-effector. The proportional and integrals gains for force control are denoted by $\mathbf{k}_{\text{p\_force}}$ and $\mathbf{k}_{\text{i\_force}}$, respectively.

In the operational space formulation, the axes assigned to force control are orthogonal to those in motion control. To specify the orthogonal directions of motion and force control tasks, the following generalized task specification matrices are used:

$$\mathbf{\Omega} = \begin{pmatrix} \mathbf{R}_{\mathcal{F}}^{\mathrm{T}} \mathbf{\Sigma}_{\mathcal{F}} \mathbf{R}_{\mathcal{F}} & \mathbf{0} \\ \mathbf{0} & \mathbf{R}_{\mathcal{M}}^{\mathrm{T}} \mathbf{\Sigma}_{\mathcal{M}} \mathbf{R}_{\mathcal{M}} \end{pmatrix}, \tag{6}$$

and

$$\bar{\mathbf{\Omega}} = \begin{pmatrix} \mathbf{R}_{\mathcal{F}}^{\mathrm{T}} \bar{\mathbf{\Sigma}}_{\mathcal{F}} \mathbf{R}_{\mathcal{F}} & \mathbf{0} \\ \mathbf{0} & \mathbf{R}_{\mathcal{M}}^{\mathrm{T}} \bar{\mathbf{\Sigma}}_{\mathcal{M}} \mathbf{R}_{\mathcal{M}} \end{pmatrix}. \tag{7}$$

$\mathbf{R}_{\mathcal{F}}$ represents the rotation matrix associated with translation/force and $\mathbf{R}_{\mathcal{M}}$ represents the rotation matrix associated with rotation/moment. These rotation matrices are needed when the desired task is specified in a frame different from the operational space frame. The selection matrix associated with translation/force at the end-effector frame is denoted $\mathbf{\Sigma}_{\mathcal{F}}$ and that associated with rotation/moment is denoted $\mathbf{\Sigma}_{\mathcal{M}}$. These selection matrices ($\mathbf{\Sigma}_{\mathcal{F}}$ and $\mathbf{\Sigma}_{\mathcal{M}}$) are 3×3 diagonal matrices whose diagonal elements are composed of 0's and 1's. A value of 1 indicates that the corresponding direction is motion controlled, while a value of 0 indicates force control. The symbol ($\bar{}$) above a parameter indicates a binary complement of that parameter.

Thus, the combined manipulator end-effector motion and force can be expressed as

$$\mathbf{F}_{\text{total}} = \mathbf{F}_{\text{motion}} + \mathbf{F}_{\text{force}}, \tag{8}$$

where the generalized selection matrix for motion is the binary complement of the generalized selection matrix for force as used in the respective motion and force equations,

$$\mathbf{F}_{\text{motion}} = \hat{\mathbf{\Lambda}}(\mathbf{x}) \mathbf{\Omega} \mathbf{F}^*_{\text{motion}} + \hat{\boldsymbol{\mu}}(\mathbf{x}, \dot{\mathbf{x}}) + \hat{\mathbf{p}}(\mathbf{x}), \tag{9}$$

$$\mathbf{F}_{\text{force}} = \hat{\mathbf{\Lambda}}(\mathbf{x}) \bar{\mathbf{\Omega}} \mathbf{F}^*_{\text{force}} + \bar{\mathbf{\Omega}} \mathbf{f}_{\text{d}}. \tag{10}$$

The torque sent to the joint motors is the combined manipulator end-effector motion and force multiplied by the transpose of the manipulator Jacobian matrix

$$\mathbf{\Gamma} = \mathbf{J}^{\mathrm{T}}(\mathbf{q}) \mathbf{F}_{\text{total}}. \tag{11}$$

The accuracy of the dynamics model is one of the most important requirements that needs to be satisfied to be able to successfully implement the operational space formulation. A number of methods have been described to identify the dynamics

Downloaded by [Botswana International University of Science & Technology (BIUST)] at 03:34 20 October 2017

parameters of a robot which include direct measurement of the dynamic parameters [14–17], a sequential identification of these parameters [18–20], moving through trajectories that excite identifiable parameters [21–23] and rule-based approach to dynamics identification [24–27]. Treatment of the robot dynamics parameters at the object-level framework is shown in Ref. [28]. In this work, the dynamics of the PUMA 560 was derived symbolically and simplified using MATHEMATICA software programmed to run the Lagrange–Euler Formulation [29]. The accuracy of the algorithm for deriving the symbolic model of the full dynamics was verified against the Matlab Robot Toolbox [30].

2.1. Singularity handling

Singularity, if not properly addressed, reduces a manipulator's usable workspace. In our application, singularity has to be addressed in both motion and force control. Usable workspace is also to be maximized. For this reason, the methods of avoiding singular configurations are not adopted. Instead we employ a singularity handling method by taking into account the lost degrees of freedom when in the singular region. A singular region is a region defined in the vicinity of a singular configuration in which a singularity robust algorithm is applied. At the exact point of singularity, the Jacobian matrix will be degenerate (or singular) and its inverse non-existent. While inside the singular region, the inverse of the Jacobian matrix is unbounded and results in an infinite joint rate for a finite task space velocities. In these configurations, the Jacobian matrix is rank-deficient and will not be able to operate in its full dofs — in the case of our robot (PUMA 560) it now possesses less than its usual 6 dofs.

We employ a method that eliminates the degenerate row of the Jacobian matrix [31], thereby reducing the dof of the task and making the robot redundant with respect to the reduced task. We first identify the singular configurations of a manipulator. When the end-effector enters a singular region, the singular configuration associated with the region is identified and the task space is transformed onto the frame of singularity $\mathbf{S}_{\mathcal{S}\mathrm{g}}(\mathbf{Sg}, x_{\mathcal{S}\mathrm{g}}, y_{\mathcal{S}\mathrm{g}}, z_{\mathcal{S}\mathrm{g}})$ with origin **Sg** and axes $x_{\mathcal{S}\mathrm{g}}$, $y_{\mathcal{S}\mathrm{g}}$ and $z_{\mathcal{S}\mathrm{g}}$. This includes transforming the Jacobian matrix and the generalized forces $\mathbf{F}_{\mathrm{total}}$, $\mathbf{F}_{\mathrm{motion}}$ and $\mathbf{F}_{\mathrm{force}}$ to the frame of singularity. The frame of singularity is the frame in which one of the axes is aligned with the direction of singularity. This represents the direction of mobility that the manipulator loses. There are several ways to identify the singular directions. We choose the Singular Value Decomposition because of its generality and completeness. In brief, the Singular Value Decomposition of the Jacobian matrix is expressed as:

$$SVD(\mathbf{J}(\mathbf{q})) = \mathbf{U}\boldsymbol{\Sigma}\mathbf{V}^{\mathrm{T}}. \tag{12}$$

$\mathbf{U} \in \mathbb{R}^{m\times m}$ and $\mathbf{V} \in \mathbb{R}^{n\times n}$ are proper orthogonal matrices and $\boldsymbol{\Sigma} \in \mathbb{R}^{m\times n}$ is a diagonal matrix with values $(\sigma_1, \sigma_2, \ldots, \sigma_m)$ [32], where $\sigma_1 \geqslant \sigma_2 \geqslant \cdots \geqslant \sigma_m \geqslant 0$ are the singular values of the matrix.

Downloaded by [Botswana International University of Science & Technology (BIUST)] at 03:34 20 October 2017

When singularity occurs, the smallest value(s) of σ_k is zero. This causes $\mathbf{\Sigma V}^T$ to be an $m \times n$ matrix (of the same dimension of the Jacobian matrix) with a row of zero, representing the direction of singularity of the manipulator. Treating $\mathbf{U}$ as a rotational matrix, then it can be used to transform the task space into the frame of singularity:

$$^{\mathcal{S}g}\mathbf{J} = \mathbf{U}^T\mathbf{J} = \mathbf{\Sigma V}^T. \tag{13}$$

After the Jacobian matrix is expressed in the frame of singularity, the direction of singularity will be reflected as a row of zeros. The degenerate component of the task is therefore eliminated by removing the zero row from the Jacobian matrix and the associated element from the generalized force vectors. The result is a Jacobian matrix that is full rank but of smaller number of rows and generalized force vectors with a reduced number of elements. The dynamics of the manipulator (which requires the inverse of the Jacobian matrix) is then calculated with the reduced Jacobian matrix but with full rank.

While inside the singular region, motion in the direction of singularity is eliminated. If motion is required in the singular direction, the end-effector can be assisted to move in such direction by the application of null space motion. Null space motion is possible inside the singular region, because one or more of the rows in the Jacobian matrix have been eliminated, which results in fewer dofs in the task space than in the joint space.

As a different control algorithm is applied inside the singular region, there is a discontinuity at the boundary of the region. This is particularly evident as the end-effector exits the singular region. Methods to smoothen out the discontinuities exist and are elaborated in Ref. [33].

2.2. Joint friction

Friction plays a significant role in robot control. When accurately modeled and used in the robot control, it could contribute to a significant improvement. The friction parameters modeled in this work are: static, kinetic or Coulomb, and fluid friction.

For each joint component of the manipulator, the friction model that is used in the force and motion control is,

$$\tau_{\text{friction}} = f_s \left(\frac{\text{sgn}(\dot{q})}{1 + \left(\frac{\dot{q}}{x_s}\right)^2} \right) + f_k \tanh(\dot{q}) + k_{vn}\dot{q}, \tag{14}$$

where f_s denotes static friction, x_s denotes a constant to correct static friction due to the Stribeck effect, f_k denotes kinetic friction, k_{vn} denotes fluid friction and $\dot{q}$ is the joint velocity. All the friction parameters have to be identified for each manipulator joint.

Downloaded by [Botswana International University of Science & Technology (BIUST)] at 03:34 20 October 2017

The total torque sent to the joint motors from equation (11) is added with the friction model to compensate for friction at each manipulator joint, that is,

$$\boldsymbol{\Gamma} = \mathbf{J}^{\mathrm{T}}(\mathbf{q})\mathbf{F}_{\mathrm{total}} + \boldsymbol{\tau}_{\mathrm{friction}}. \tag{15}$$

2.3. Impact control

Another issue needed to be addressed in this work is the transition from contact to non-contact state between the end-effector of the manipulator and its environment. We employ impact loading control [34] to create a smooth transition between the two states. The key idea is to quickly dissipate the impact force using a motion command:

$$\mathbf{F}^{*}_{\mathrm{motion}} = -\mathbf{k}_{\mathrm{v\_motion}}\dot{\mathbf{x}}. \tag{16}$$

Note that the $\mathbf{F}^{*}_{\mathrm{motion}}$ is different from equation (2).

3. IMPLEMENTATION

After the derivation of the full dynamics model and the identification of its parameters, the operational space formulation is ready for implementation. Several stages of implementation were performed before finally arriving at simultaneous force and motion control.

3.1. Gravity compensation on force/torque sensor reading

For the purpose of cancelling the gravity effect on the manipulator arm, the mass and center of mass model of the manipulator is fed forward. This stage verifies the accuracy of the mass and center of mass for each link of the manipulator. With a 'floating' manipulator, the human operator can move the manipulator links to anywhere within its workspace with minimal effort. This has a direct application in walk-through programming for welding robots [35].

Gravity compensation in the force reading is important in the polishing task, as one would like to decouple the weight of the polishing tool from the contact forces with the environment. The force sensor frame is denoted by $\mathbf{S}_{\mathcal{S}}(\mathcal{S}, x_{\mathrm{s}}, y_{\mathrm{s}}, z_{\mathrm{s}})$ with origin $\mathcal{S}$ and axes x_{s}, y_{s} and z_{s} (see Fig. 2). A force/torque sensor provides readings of forces/torques acting on the sensor frame, with respect to the sensor frame itself. A sensor reading of the force/torque applied by the manipulator on its environment, with the weight of the tool removed, is denoted ${}^{\mathrm{s}}\mathbf{f}_{\mathrm{s}}$. It can be expressed as

$${}^{\mathrm{s}}\mathbf{f}_{\mathrm{s}} = {}^{\mathrm{s}}\mathbf{f}_{\mathrm{raw}} + {}^{\mathrm{s}}\mathbf{f}_{\mathrm{gravity}} - {}^{\mathrm{s}}\mathbf{f}_{\mathrm{offset}}, \tag{17}$$

where ${}^{\mathrm{s}}\mathbf{f}_{\mathrm{raw}}$ is the negative of the total force/torque applied by the environment on the manipulator's end-effector (including gravitational effects), ${}^{\mathrm{s}}\mathbf{f}_{\mathrm{gravity}}$ is the model

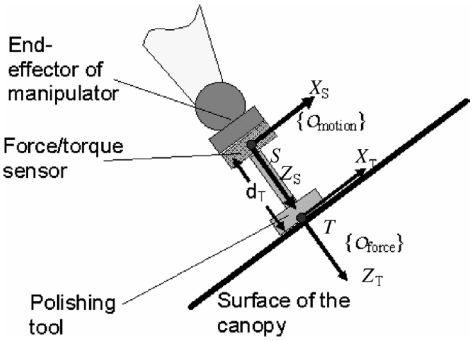

Figure 2. The choice of operational point for simultaneous force and motion control. The motion control operational point ($\mathcal{O}_{\text{motion}}$) was specified to be at the center of the force/torque sensor (point S), while the force control operational point ($\mathcal{O}_{\text{force}}$) was placed at the center of the face of the polishing tool tip (point T). The orientation of frames S and T are the same.

of the gravitational force/torque that is added in order to correct the gravitational forces acting on the force/torque sensor and ${}^{\text{s}}\mathbf{f}_{\text{offset}}$ is the force/torque offset used by most sensors to automatically zero out the current sensor reading upon activation.

To model the gravitational term, ${}^{\text{s}}\mathbf{f}_{\text{gravity}}$, the manipulator's end-effector is assumed to be at initialization when the necessary corrections were made, that is, facing upward. The gravitational model is computed by expressing the gravitational force at the polishing tool's center of mass, ${}^{0}\mathbf{f}_{\text{m}}$, with respect to the base frame (0) and changing its reference frame to that of the force sensor frame (S), that is,

$$ {}^{\text{s}}\mathbf{f}_{\text{gravity}} = {}^{\text{s}}\mathbf{J}^{*}_{\text{m}}\, {}^{\text{m}}\mathbf{J}^{*}_{0}\, {}^{0}\mathbf{f}_{\text{m}}, \tag{18} $$

where ${}^{0}\mathbf{f}_{\text{m}}$ is the gravitational force at the center of mass of the polishing tool expressed with respect to the base frame and is computed as ${}^{0}\mathbf{f}_{\text{m}} = [0\ \ 0\ \ m_{\text{tool}}g\ \ 0\ \ 0\ \ 0]^{\text{T}}$. The total mass of the polishing tool $m_{\text{tool}} = 1.8$ kg and the gravitational constant $g = 9.81\ \text{m/s}^2$. The orientation of the tool frame is coincident with the orientation of the sensor frame. Thus the transformation matrix ${}^{\text{s}}\mathbf{J}^{*}_{\text{m}}$ changes the reference frame from the tool to the sensor by taking into account only the distance between the origin of the two frames,

$$ {}^{\text{s}}\mathbf{J}^{*}_{\text{m}} = \begin{pmatrix} \mathbf{I} & \mathbf{0} \\ \lfloor {}^{\text{s}}\mathbf{p}_{\text{m}} \times \rfloor & \mathbf{I} \end{pmatrix}, \tag{19} $$

where ${}^{\text{s}}\mathbf{p}_{\text{m}}$ is the position vector of the tool's center of mass with respect to the sensor frame such that

$$ \lfloor {}^{\text{s}}\mathbf{p}_{\text{m}} \times \rfloor = \begin{bmatrix} 0 & -{}^{\text{s}}p_{\text{m}z} & {}^{\text{s}}p_{\text{m}y} \\ {}^{\text{s}}p_{\text{m}z} & 0 & -{}^{\text{s}}p_{\text{m}x} \\ -{}^{\text{s}}p_{\text{m}y} & {}^{\text{s}}p_{\text{m}x} & 0 \end{bmatrix}, \tag{20} $$

Downloaded by [Botswana International University of Science & Technology (BIUST)] at 03:34 20 October 2017

Downloaded by [Botswana International University of Science & Technology (BIUST)] at 03:34 20 October 2017

where ${}^{\mathrm{s}}p_{\mathrm{m}x}$, ${}^{\mathrm{s}}p_{\mathrm{m}y}$ and ${}^{\mathrm{s}}p_{\mathrm{m}z}$ are the x, y and z components of the vector ${}^{\mathrm{s}}\mathbf{p}_{\mathrm{m}}$, respectively. The transformation matrix ${}^{\mathrm{m}}\mathbf{J}_0^*$ can be derived from the transformation matrix ${}^{\mathrm{s}}\mathbf{J}_0^*$

$$ {}^{\mathrm{s}}\mathbf{J}_0^* = \begin{bmatrix} {}^{\mathrm{s}}\mathbf{R}_0 & \mathbf{0} \\ \mathbf{0} & {}^{\mathrm{s}}\mathbf{R}_0 \end{bmatrix}, \tag{21} $$

since the sensor frame orientation is the identical to the tool frame orientation. ${}^{\mathrm{s}}\mathbf{R}_0$ is the orientation of the base frame, $\mathbf{S}_0(\mathbf{0}, x_0, y_0, z_0)$, with respect to the sensor frame, $\mathbf{S}_{\mathcal{S}}(\mathcal{S}, x_{\mathrm{s}}, y_{\mathrm{s}}, z_{\mathrm{s}})$. The orientation of the sensor frame is identical to the orientation of the end-effector frame which makes ${}^{\mathrm{s}}\mathbf{R}_0 = {}^{0}\mathbf{R}_{\mathrm{e}}^{\mathrm{T}}$.

3.2. Motion and force control

The operational point for motion control ($\mathcal{O}_{\mathrm{motion}}$) was chosen to be at the center of the force/torque sensor (see Fig. 2). Due to the higher degree of flexibility of the polishing tool compared to the links of the PUMA manipulator, choosing the operational point for motion control closer to the wrist point helps keep the compliant motion robust, as less effort is needed in controlling the posture of the manipulator. The desired motion at the wrist is transformed to $\mathcal{O}_{\mathrm{motion}}$ through the appropriate transformation matrix and motion control is performed by tracking the desired trajectory at this point. The robot control is based on the dynamics of rigid bodies and the higher degree of flexibility of the polishing tool create higher penalty on the motion control.

A PI controller is set up to regulate force control (equations (4) and (5)). The compliant motion of the manipulator, adjusting its pose such that its end-effector is always normal to the surface of the workpiece being polished, is created by setting the desired moment to zero around the x_t and y_t axes of the end-effector frame $\mathbf{S}_{\mathcal{T}}(T, x_t, y_t, z_t)$ (see Fig. 2). Due to the high frequency noise of the force/torque sensor reading, a derivative controller was found to introduce too much instability. A PI controller was chosen instead.

The operational point of the force controller ($\mathcal{O}_{\mathrm{force}}$) was placed at the center of polishing tool tip, in contact with the surface of the workpiece/environment (point T, see Fig. 2). One advantage of this choice is that it allows compliance of the whole robot structure as a response to the interaction force and moment with the environment at the end-effector. Another advantage is that it eliminates the ambiguity of the moment reading which is present if the operational point was placed at the center of the force/torque sensor itself (point S). By ambiguity, we mean that a reading for moments at the force/torque sensor (around x_{s} and y_{s} axes of the sensor frame), could mean two things. The first is the moment created by the polishing tool's friction with the surface of the workpiece, as it moves along the surface (a moment reading around x_{s} axis of the end-effector frame is created by motion in the y_{s} direction and *vice versa*). The second is due to the need for compliant motion, as the curvature of the workpiece surface changes. Placing the operational point at the center of the polishing tool, in contact with the surface of

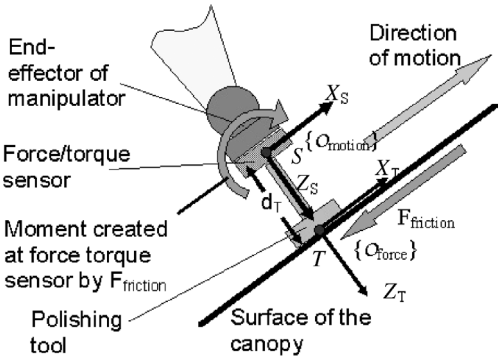

Figure 3. Friction force $\mathbf{F}_{\text{friction}}$ causes a moment reading to be registered at the force/torque sensor (point S), but creates no moment at point T ($\mathcal{O}_{\text{force}}$).

the workpiece means that the frictional forces between the surfaces ($\mathbf{f}_{\text{friction}}$) would generate no resultant moment around the operational point ($\mathcal{O}_{\text{force}}$) (see Fig. 3).

The forces at the tooltip can be computed from the force sensor reading using the following transformation:

$$^{\text{T}}\mathbf{f}_{\text{T}}^{*} = \begin{pmatrix} \mathbf{I} & \mathbf{0} \\ \lfloor {}^{\text{S}}\mathbf{p}_{\text{T}} \times \rfloor & \mathbf{I} \end{pmatrix} {}^{\text{S}}\mathbf{f}_{\text{S}}, \tag{22}$$

where ${}^{\text{s}}\mathbf{p}_{\text{T}}$ is the position vector of the operational point T with respect to the sensor frame. The term $\lfloor {}^{\text{S}}\mathbf{p}_{\text{T}} \times \rfloor$ is a skew symmetric matrix as defined in equation (20).

3.3. Specifying direction for motion and force control

Following the explanation in Section 3.2, in the polishing task, the operational point for motion control is set to be the center of the force/torque sensor ($\mathcal{O}_{\text{motion}}$), while that for force control is at the center of the polishing tool surface which is in contact with the workpiece ($\mathcal{O}_{\text{force}}$, see Figs 2 and 3). Although the origins of the two reference frames are not coincident, the directions of their respective axes are the same. Thus, by specifying a direction to be under force control, the corresponding motion control in the same direction is disabled.

Force is controlled in the direction of the z_t-axis (see Fig. 3). In the polishing task, the z_t-axis is the instantaneous normal to the canopy surface as the robot end-effector moves along the surface. The desired normal force to be exerted on the surface of the environment is specified along the z_t-axis. Moment is controlled about the x_t- and y_t-axes. Motion control is specified along the remaining axes that are not under force/moment control: position control along the x_t- and y_t-axes and orientation control about the z_t-axis. This results in the following selection matrices ($\mathbf{\Sigma}_{\mathcal{F}}$ and $\mathbf{\Sigma}_{\mathcal{M}}$):

$$\mathbf{\Sigma}_{\mathcal{F}} = \begin{pmatrix} 1 & 0 & 0 \\ 0 & 1 & 0 \\ 0 & 0 & 0 \end{pmatrix}, \tag{23}$$

Downloaded by [Botswana International University of Science & Technology (BIUST)] at 03:34 20 October 2017

$$\mathbf{\Sigma}_{\mathcal{M}} = \begin{pmatrix} 0 & 0 & 0 \\ 0 & 0 & 0 \\ 0 & 0 & 1 \end{pmatrix}. \tag{24}$$

3.4. Singularity handling

In our application, where a PUMA 560 robot was used, there are three singularity configurations: head, elbow and wrist singularities. The most critical one is the wrist singularity, as it happens when the wrist is straightened and it is a frequently occurring configuration. Elbow and head singularities never occur in our polishing application.

For the example of wrist singularity of PUMA 560 used in our application, the singular configuration is identified by taking the determinant of the Jacobian matrix as the configuration where the wrist is straightened ($q_5 = 0$). The singular region is defined as:

$$|q_5| \leqslant q_{5t}, \tag{25}$$

where q_{5t} is the threshold value of the joint.

In the case of the wrist singularity, null space motion is utilized to smooth out the discontinuity by keeping the singular direction away from the desired trajectory. The null space motion creates internal joint motion that shifts the direction of singularity. While inside the singular region, a potential function is defined so that the direction of singular is perpendicular to the desired path. This also has the additional effect of ensuring that the end-effector moves along, and exits the singular region through, a controllable axis of motion, which is orthogonal to the direction of singularity. Hence, no discontinuity occurs at the boundary of the singular region. Details are given in Ref. [33].

3.5. Joint friction

The fluid friction parameters are identified together with the manipulator dynamics as discussed in [20]. On the other hand, static and kinetic friction parameters were derived using the methods discussed in [36]. The values of the friction parameters that were derived are shown in Table 1.

Table 1.
Friction parameters of PUMA 560

Link	f_s	f_k	k_{vn}	x_s
1	5	2	1	0.1
2	5	2	1	0.1
3	2.5	1	1	0.1
4	0.3	0.1	0.05	0.1
5	0.2	0.1	0.05	0.1
6	0.2	0.1	0.05	0.1

Downloaded by [Botswana International University of Science & Technology (BIUST)] at 03:34 20 October 2017

Downloaded by [Botswana International University of Science & Technology (BIUST)] at 03:34 20 October 2017

3.6. Impact control

In the overall canopy polishing task, the mobile manipulator undergoes three stages:

- the end-effector approaches the canopy using motion control;
- then it establishes contact with the canopy surface and dissipates the force of impact using impact loading and control;
- and lastly, it performs the polishing task using unified force and motion control.

At stage 1, the operator roughly guides the mobile manipulator to a location so that it faces the workpiece (the canopy to be polished) and a command to move the end-effector forward towards the surface is given in order to establish a contact between the polishing tool and the canopy surface. Since this stage uses motion control, the selection matrices $\Sigma_{\mathcal{F}}$ and $\Sigma_{\mathcal{M}}$ are set to identity and the motion control law in equation (2) is used. Throughout this motion, force is monitored along the z_t-axis of the end-effector frame $\mathbf{S}_{\mathcal{T}}(T, x_t, y_t, z_t)$ with a threshold of 10 N. When the polishing tool collides with the canopy, a force along z_t-axis that is way above the threshold is sensed. The manipulator would then enter into the second stage using impact loading and control. Here, equation (16) is used instead of equation (2), in order to dissipate the impact of collision between the tool and the aircraft canopy. After the impact has been dissipated and the force along z_t-axis goes below the threshold value of 10 N, the manipulator commences the polishing algorithm (stage 3).

4. IMPLEMENTATION RESULTS

Data of the mobile manipulator responses at the different stages of the aircraft canopy polishing task are presented in this section. Graphs are shown for the following robot responses during motion control, during simultaneous force and motion control while performing the polishing task, variation in force reading while polishing within the singularity region, force profile measured during impact and force dissipation, and the effect of friction modeling on the performance of the system in the polishing task.

In this work, although the PUMA 560 is physically attached to the XR4000 mobile base, the controller of the manipulator arm is not integrated with the controller of the mobile base. Thus, the manipulator arm and the mobile base are independently controlled. Throughout this work, the operational space formulation applies only to the manipulator arm while the mobile base is controlled *via* a joystick. Thus the human operator's random motion of the mobile base is considered purely as disturbance to the polishing task.

A JR3 six-axes force/torque sensor is attached on the face of the sixth link of the arm. Then on the other end of the force/torque sensor, a grinder tool with a rated speed of 10 000 rpm is attached. The grinder tool, which weighs about 1.8 kg, has been accurately compensated for gravity on the force/torque sensor reading. The end-effector exerts the required instantaneous normal force of 10 N on the

Downloaded by [Botswana International University of Science & Technology (BIUST)] at 03:34 20 October 2017

canopy surface. During canopy polishing, the mobile base was randomly moved by the human operator *via* a joystick at an average speed of 0.5 m/s. Emphasis on the implementation results is focused on how well the manipulator arm's end-effector achieved the desired normal force on the canopy surface while moving in a compliant behavior with base disturbances created by the random motion of the mobile base and the end-effector disturbances created by the running grinder.

4.1. Motion control in operational space

After the verification of a correct robot response on gravitational force compensation where the manipulator arm floats against forces of gravity, the motion control verifies the correctness of the inertial parameters of the full dynamics model. Motion control is admittedly less sensitive to errors in the model and control of a manipulator compared to a combined force and motion control. However, by specifying a higher precision in the robot response in motion control with the robot running at higher speeds, a manipulator can be determined to have achieved the desired level of accuracy. To this end, the PUMA was put to an extreme test. Shown in Fig. 4 is the error in the PUMA response as it moved with motion control in all six degrees-of-freedom operational space. The PUMA is tasked to move 1 m in 1 s along the base frame axis y_0 (horizontal) with fixed end-effector orientation facing downward. To achieve these goal parameters, the PUMA end-effector reached a maximum speed of 1.9 m/s.

Position errors are shown as X_err, Y_err, and Z_err in units of meters, while orientation errors are shown as DPhi[1], DPhi[2], and DPhi[3] in units of radians.

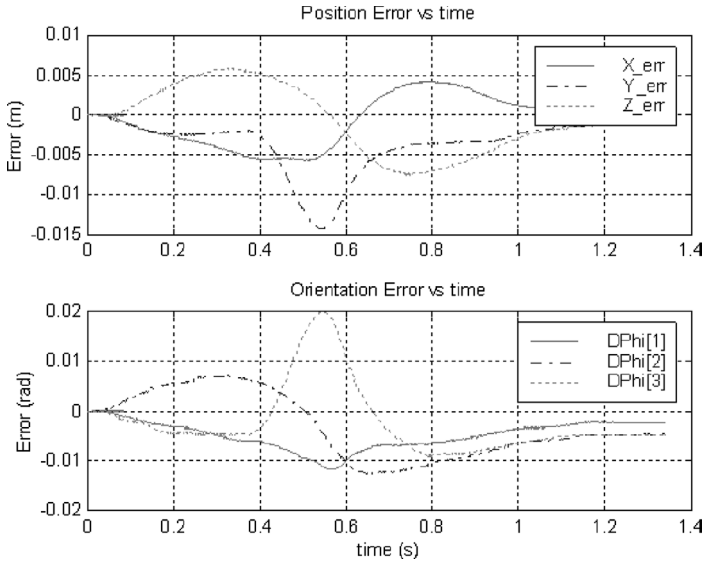

Figure 4. Error response of the PUMA arm in motion control with its end-effector running at a maximum speed of 1.9 m/s.

Downloaded by [Botswana International University of Science & Technology (BIUST)] at 03:34 20 October 2017

Maximum position error is along the y_0-axis, being 0.014 m. One possible cause of this relatively significant error could be the saturation of the joint motors at the maximum end-effector speed. The orientation error is derived from the cross product of the actual and desired orientation vectors **n**, **o** and **a** as stated in Ref. [37], that is,

$$\delta\Phi = \frac{1}{2}\big((\mathbf{n}_\mathrm{a} \times \mathbf{n}_\mathrm{d}) + (\mathbf{o}_\mathrm{a} \times \mathbf{o}_\mathrm{d}) + (\mathbf{a}_\mathrm{a} \times \mathbf{a}_\mathrm{d})\big), \tag{26}$$

where **n**, **o** and **a** are columns of an orientation matrix expressing the orientation of the end-effector with respect to the base, that is, ${}^0\mathbf{R}_\mathrm{e} = [\mathbf{n}\ \mathbf{o}\ \mathbf{a}]$ and the subscripts a and d refer to actual and desired parameters. Maximum orientation error is around the z_0-axis which is 0.02 radians.

4.2. Simultaneous force and motion control

The PUMA end-effector was specified to run a non-terminating sinusoidal path along the y_t-axis of the end-effector frame $\mathbf{S}_\mathcal{T}(T, x_t, y_t, z_t)$, with respect to the base frame, with an amplitude of 0.15 m and a period of 5 s.

An inherent disturbance to the PUMA is the motion of the grinder attached to its end-effector (rated at 10 000 rpm). The other disturbance is at the PUMA's base where the independently controlled XR4000 is randomly moved by the human operator *via* a joystick in order to move the whole mobile manipulator to give its end-effector access to desired areas on the canopy. The PUMA response for simultaneous force and motion control with the given disturbances is shown in Fig. 5.

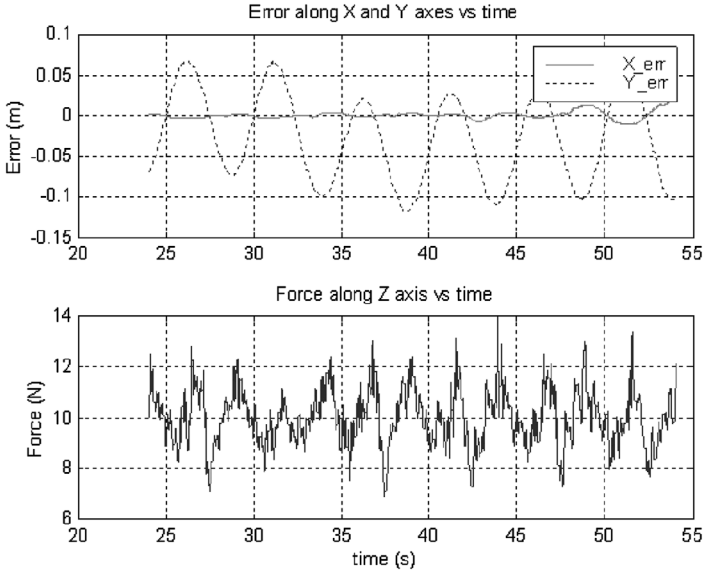

Figure 5. Error response of the PUMA doing polishing on the aircraft canopy with 10 N desired normal force and with Nomad base moving.

Downloaded by [Botswana International University of Science & Technology (BIUST)] at 03:34 20 October 2017

The maximum position error along the direction of motion (y_t-axis of the frame $\mathbf{S}_{\mathcal{T}}(T, x_t, y_t, z_t)$) and is at 0.12 m, compared to 0.07 m when the polishing was done with a stationary base. The maximum force error along the z_t-axis of the frame $\mathbf{S}_{\mathcal{T}}(T, x_t, y_t, z_t)$ is 4 N, compared to about 3.2 N when the base is stationary. The main source of error in the tracking performance is the unmodeled friction between the polishing tool and the surface of the canopy. This causes a lag in the end-effector's tracking of the desired trajectory. This lag is not critical in our application as we only need to polish around the area.

4.3. Force reading around the region of singularity

Compared to position errors, force errors in a robot response are more sensitive to non-smooth transitions in the robot control. Thus, the robustness of the singularity handling algorithm presented in this work is tested by the letting the PUMA polish the aircraft canopy as it goes in and out of the wrist singularity region (Fig. 6) and the normal force exerted on the canopy is observed. The results are shown in Fig. 7.

The PUMA is set to move along the x_t-axis of the end-effector frame $\mathbf{S}_{\mathcal{T}}(T, x_t, y_t, z_t)$ with respect to the stationary base frame. As the PUMA performed its polishing task in a sinusoidal path, it crosses the singular configuration every time the wrist is straightened (see Fig. 6), the determinant of the Jacobian is recorded to monitor its proximity with respect to singularity (Fig. 7). A value of zero for the determinant of the Jacobian is a point of singularity. The desired normal force on the canopy surface is set to the same value of 10 N. Around the region of singularity, the

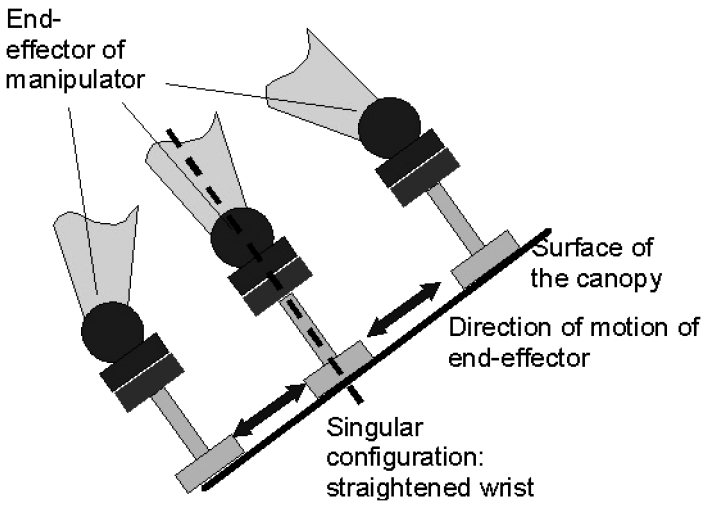

Figure 6. The experimental setup where PUMA is to move sinusoidally about the wrist singularity, while performing motion and force control. The singular configuration is when the wrist is straightened.

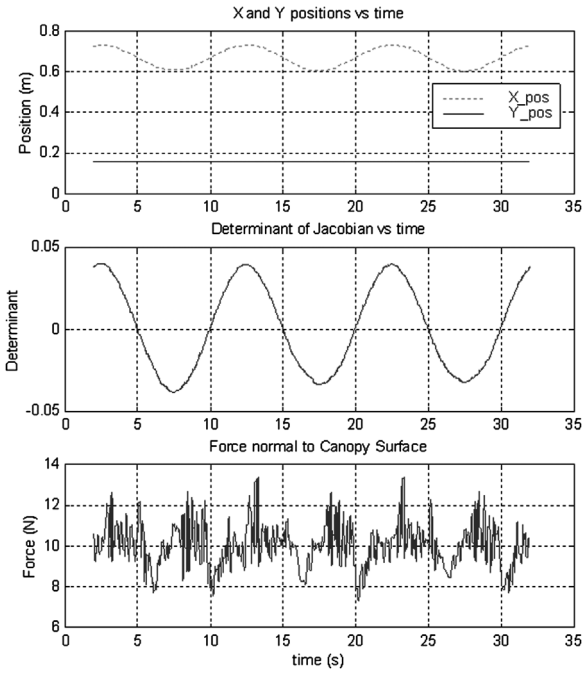

Figure 7. Force reading exerted by PUMA normal to the aircraft canopy surface at it moves in and out of wrist singularity region.

maximum force error reading is 3.7 N, without any significant difference from the maximum of 3.2 N when polishing was done with a stationary base without going through singular configuration.

4.4. Force dissipation on impact

Figure 8 shows the results for impact loading and control. As the PUMA end-effector approached the canopy surface, force was monitored along the z_T-axis of the end-effector frame $\mathbf{S}_T(T, x_t, y_t, z_t)$ with respect to the same frame. A threshold of 10 N was used to determine the instance of impact and the dissipation of impact forces. As soon as impact was detected, impact loading control was performed using equation (16). As the impact forces were dissipated, the PUMA then started its polishing task.

4.5. Manipulator response with and without friction compensation

The comparison of the end-effector force exerted normal to the canopy surface with and without compensating friction parameters while the manipulator is performing its polishing task is shown in Fig. 9. Notice the difference in time when the force data were taken. This is because the data was taken on exactly the same experimental setup noting the fact that friction parameters are dependent on ambient condition. On the first set of data, the PUMA polished the canopy without friction

Downloaded by [Botswana International University of Science & Technology (BIUST)] at 03:34 20 October 2017

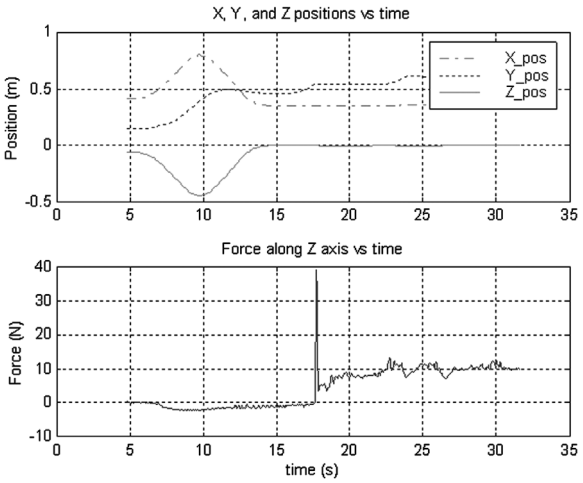

Figure 8. Force reading exerted by PUMA normal to the aircraft canopy surface before, during and immediately after impact loading.

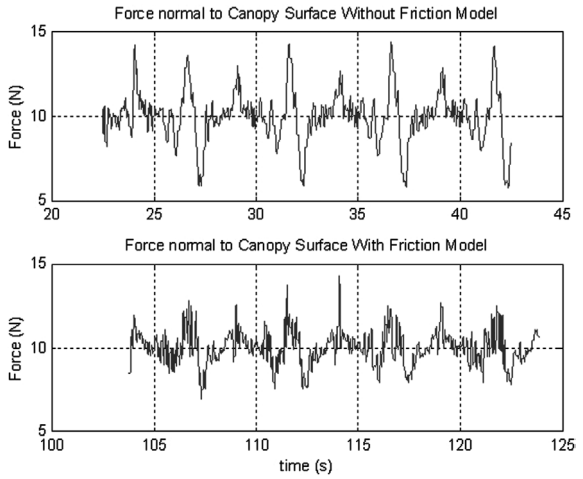

Figure 9. Comparison on the force reading exerted by PUMA normal to the aircraft canopy surface with and without friction model.

model and the force response was recorded. Then, as it continued to perform the polishing task the friction model was introduced, after which the next set of force responses were recorded. It was observed that friction compensation was able to reduce maximum force tracking error by up to 32%.

5. CONCLUSIONS

It has been shown in this implementation that robust simultaneous force and motion control is possible for a mobile manipulator set-up where the manipulator arm,

Downloaded by [Botswana International University of Science & Technology (BIUST)] at 03:34 20 October 2017

Downloaded by [Botswana International University of Science & Technology (BIUST)] at 03:34 20 October 2017

a PUMA 560, is controlled independent of the mobile base, a Nomad XR4000. The full dynamics of the PUMA are modeled and it is controlled using the operational space formulation. The PUMA performed the polishing task subject to end-effector disturbances due to the attached grinder running at a rated speed of 10 000 rpm plus base disturbances due to the human operator randomly moving the mobile base at an average speed of 0.5 m/s. The polishing task was performed with the end-effector exerting a normal force of 10 ± 4 N on the canopy surface and moving in a compliant motion on the curved canopy surface that is of unknown geometry. Further work would be focused in implementing a fully integrated mobile manipulator with it a full dynamic model of the combined mobile manipulator system.

Acknowledgements

The financial support of Singapore Institute of Manufacturing Technology in this collaborative research project is gratefully acknowledged.

REFERENCES

1. D. E. Whitney, Historical perspective and state of the art in robot force control, *Int. J. Robot. Res.* **6** (1), 3–14 (1987).
2. M. H. Raibert and J. J. Craig, Hybrid position/force control of manipulators, *ASME J. Dyn. Syst., Meas., Contr.* **103** (2), 126–133 (1981).
3. O. Khatib, A unified approach for motion and force control of robot manipulators: The operational space formulation, *IEEE J. Robot. Automat.* **RA-3** (1), 43–53 (1987).
4. J. K. Mills and A. A. Goldenberg, Force and position control of manipulators during constrained motion and tasks, *IEEE Trans. Robot. Automat.* **5** (1), 30–46 (1989).
5. R. P. C. Paul and B. Shimano, Compliance and control, in: *Proc. Joint Automat. Contr. Conf.*, San Francisco, CA, pp. 694–699 (1976).
6. M. T. Mason, Compliance and force control for computer controlled manipulators, *IEEE Trans. Syst., Man, Cybern.* **SMC-11** (6), 418–432 (1981).
7. L. L. Whitcomb, S. Arimoto, T. Naniwa and F. Ozaki, Adaptive model-based hybrid control of geometrically constrained robot arms, *IEEE Trans. Robot. Automat.* **13** (1), 105–116 (1997).
8. N. Hogan, Impedance control: An approach to manipulation, *ASME J. Dyn. Syst., Meas., Contr.* **107** (1), 1–24 (1985).
9. H. Kazerooni, On the robot compliant motion control, *ASME J. Dyn. Syst., Meas., Contr.* **111** (3), 416–425 (1989).
10. J. K. Salisbury, Active stiffness control of a manipulator in cartesian coordinates, in: *Proc. 19th IEEE Conf. Decision Contr.*, Albuquerque, NM, Vol. 1, pp. 95–100 (1980).
11. M. Pelletier and L. K. Daneshmend, An approach to compliant motion planning using uncertain impedance models, in: *Proc. IASTED Int. Conf. Contr. Robot.*, Vancouver, pp. 58–61 (1992).
12. O. Khatib, Commande dynamique dans l'espace operationnel des robots manipulateurs en presence d'obstacles, PhD dissertation, Ecole Nationale Superieure de l'Aeronautique et de l'Espace, Toulouse (1980) (in French).
13. D. Oetomo, M. H. Ang, Jr. and T. M. Lim, Haptic interface for force/motion controlled mobile manipulator, in: *Proceedings of the 2nd IFAC Conference on Mechatronic Systems*, Berkeley, CA, pp. 566–571 (2002).
14. A. K. Bejczy, Robot arm dynamics and control, *Technical Memo* **33** (669) (1974).

Downloaded by [Botswana International University of Science & Technology (BIUST)] at 03:34 20 October 2017

15. R. Paul, M. Rong and H. Zhang, Dynamics of puma manipulator, in: *Proc. Am. Control Conf.*, San Francisco, CA, pp. 491–496 (1983).
16. T. J. Tarn, A. K. Bejczy, S. Han and X. Yun, Inertia parameters of PUMA 560 robot arm, Technical Report, Volume SSM-RL-85-01 (1985).
17. B. Armstrong, O. Khatib and J. Burdick, The explicit dynamic model and inertial parameters of the PUMA 560 arm, in: *Proc. IEEE Int. Conf. Robot. Automat.*, San Francisco, CA, pp. 510–518 (1986).
18. M. Renaud, An efficient iterative analytic procedure for obtaining a robot manipulator dynamic model, *Int. J. Robot. Res.* **3**, 749–764 (1984).
19. J. J. Curtelin, Sequential identification of the dynamic parameters of a robot, in: *Proc. 5th Int. Conf. Adv. Robot.*, Pisa, Italy, pp. 1513–1516 (1991).
20. R. Jamisola, M. H. Ang, Jr., T. M. Lim, O. Khatib and S. Y. Lim, Dynamics identification and control of an industrial robot, in: *Proc. 9th Int. Conf. Adv. Robot.*, Tokyo, Japan, pp. 323–328 (1999).
21. B. Armstrong-Hélouvry, On finding 'exciting' trajectories for identification experiments involving systems with non-linear dynamics, *Int. J. Robot. Res.* **8** (6), 28–48 (1989).
22. P. K. Khosla, Categorization of parameters in the dynamic robot model, *IEEE J. Robot. Automat.* **5** (3), 261–268 (1989).
23. J. Swevers, C. Ganseman, D. B. Tukel, J. D. Schutter and H. V. Brussel, Optimal robot excitation and identification, *IEEE Trans. Robot. Automat.* **13** (5), 730–740 (1997).
24. R. Lucyshyn and J. Angeles, A rule-based framework for parameter estimation of robot dynamic models, in: *Proc. Int. Conf. Intell. Robots Syst.*, Osaka, Vol. 2, pp. 745–750 (1991).
25. K. Yuan, C. Wang and L. Yan, A new approach to parameter identification of robot manipulators, in: *Proc. IEEE Int. Conf. Ind. Tech.*, pp. 92–96 (1994).
26. A. Y. Zomaya, Extraction and computation of identifiable parameters in robot dynamic models: theory and application, in: *IEEE Proc. Contr. Theory Appl.* **141**, 48–56 (1994).
27. P. O. Vandajon, M. Gautier and P. Desbats, Identification of robots inertial parameters by means of spectrum analysis, in: *Proc. IEEE Int. Conf. Robot. Automat.*, Nagoya, Aichi, Vol. 3, pp. 3033–3038 (1995).
28. O. Khatib, Inertial properties in robotic manipulation: An object-level framework, *Int. J. Robot. Res.* **14** (1), 19–36 (1995).
29. K. Fu, R. Gonzales and C. Lee, *Robotics: Control, Sensing, Vision, and Intelligence*. McGraw-Hill, Singapore (1987).
30. P. Corke, A robotics toolbox for matlab, *IEEE Robot. Automat. Magn.* **3** (1), 24–32 (1996).
31. D. Oetomo, M. H. Ang, Jr. and S. Y. Lim, Singularity handling on puma in operational space formulation, in: *Lecture Notes Control Inform. Sci.* **271**, 491–501 (2001).
32. T. Yoshikawa, Analysis and control of robot manipulators with redundancy, in: *Robotics Research*, M. Brady and R. Paul (Eds), pp. 735–747. MIT Press, Cambridge, MA (1984).
33. D. Oetomo and M. H. Ang, Jr., Singularity handling method with division in workspace and discontinuity issue, in: *Proc. Int. Symp. Dynam. Control*, Hanoi (2003).
34. O. Khatib and J. Burdick, Motion and force control of robot manipulators, in: *Proc. IEEE Int. Conf. Robot. Automat.*, San Francisco, CA, pp. 1381–1386 (1986).
35. M. H. Ang, Jr., W. Lin and S. Y. Lim, A walk-through programmed robot for welding in shipyards, *Ind. Robot* **26** (5), 377–388 (1999).
36. B. Armstrong-Hélouvry, *Control of Machines with Friction*. Kluwer, Boston, MA (1991).
37. J. Luh, M. Walker and R. Paul, Resolved-acceleration control of mechanical manipulators, *IEEE Trans. Automat. Contr.* **AC-25** (3), 468–474 (1980).

Downloaded by [Botswana International University of Science & Technology (BIUST)] at 03:34 20 October 2017

ABOUT THE AUTHORS

Rodrigo S. Jamisola, Jr. received the BS in Mechanical Engineering from the University of the Philippines, Diliman, in 1993. He received his Master of Engineering from National University of Singapore in 2001 and is currently a PhD student at Colorado State University. His research interests include force and motion control, and failure-tolerant motion planning for redundant robots.

Denny Oetomo received the BEng from the Australian National University in 1997 and PhD from National University of Singapore (NUS) in 2004. He worked as photolithography engineer for Hewlett Packard Singapore in 1998–1999 and as research engineer to NUS and the Singapore Institute of Manufacturing Technology in 2002–2004. He joined the Robotics and Mechatronics Research Laboratory (RMRL) at Monash University in November 2004 where he is currently a Research Fellow. His research interests include force and motion control of mechanisms, haptics and micro/nano-manipulation with flexure joints.

Marcelo H. Ang, Jr. received the BS degrees (cum laude) in Mechanical Engineering and Industrial Management Engineering from the De La Salle University, Manila, Philippines, in 1981; the MS degree in Mechanical Engineering from the University of Hawaii at Manoa, Honolulu, HI, in 1985; and the MS and PhD degrees in Electrical Engineering from the University of Rochester, Rochester, NY, in 1986 and 1988, respectively. His work experience include heading the Technical Training Division of Intel's Assembly and Test Facility in the Philippines, research positions at the East West Center in Hawaii and at the Massachusetts Institute of Technology, and a faculty position as an Assistant Professor of Electrical Engineering at the University of Rochester, NY. In 1989, Dr. Ang joined the Department of Mechanical Engineering of the National University of Singapore, where he is currently an Associate Professor. In addition to academic and research activities, he is actively involved in the Singapore Robotic Games as its founding chairman. His research interests span the areas of robotics, mechatronics, automation, computer control and applications of intelligent systems methodologies.

Oussama Khatib is Professor of Computer Science at Stanford University. He received his PhD in 1980 from Sup'Aero, Toulouse, France. His current research is in human-centered robotics, human motion synthesis, humanoid robots, dynamic simulations, haptic interactions and human-friendly robot design. His exploration in this research ranges from the autonomous ability of a robot to cooperate with a human to the haptic interaction of a user with an animated character or a surgical instrument. His research in these emerging areas builds on a large body of studies he pursued over the past 25 years and published in over 200 contributions in the field. He was Program Chair of ICRA2000 (San Francisco) and Editor of *The Robotics Review*, MIT Press. He has served as the Director of the Stanford Computer Forum, an industry affiliate program. He is currently the President of the International Foundation of Robotics Research, IFRR, and Editor of *STAR*, *Springer Tracts in Advanced Robotics*. He is an IEEE Fellow, a Distinguished Lecturer of IEEE and a recipient of the JARA Award.

Tao Ming Lim received his BEng degree (Hons) in Mechanical Engineering from National University of Singapore (NUS) in 1998. He continued to pursue his Master degree with NUS and worked as a research student in Singapore Institute of Manufacturing Technology (SIMTech). His Master research project was in Software Architecture for Real-Time Robotic Control. He joined SIMTech in 2001 after completing his Master Degree. His current research projects include the NUS-SIMTech collaborative research project in developing a robust mobile manipulator for unstructured environment and nano precision stage for 2D/3D wafer inspection system.

Ser Yong Lim received his BEng, 1st Class Honours, from the National University of Singapore in 1984, and his MSc, and PhD from Clemson University (Clemson, SC, USA), in 1988 and 1994, respectively. He has many years of working experience in the industry. In 1994, Dr. Lim joined Singapore Institute of Manufacturing Technology where he is now a Senior Scientist and Deputy Executive Director on Research. His main research interests are in nonlinear control of robotic manipulators, ultra-precision systems, force-controlled robots and real-time systems. He is now leading two research projects, one on robot dynamic control and the other on ultra-precision positioning systems.

Downloaded by [Botswana International University of Science & Technology (BIUST)] at 03:34 20 October 2017